ACS APPLIED ENERGY MATERIALS
Cite This: ACS Appl. Energy Mater. 2019, 2, 1019−1025
Article
www.acsaem.org

Highly Efficient Benzo-Furan-Based Electron Acceptor Derived from One-Pot Synthesis for High-Performance Bulk Heterojunction Solar Cells

P. Nagarjuna,[†,‡] Anirban Bagui,[†] Ravulakollu Srinivasa Rao,[†,‡] Vinay Gupta,[*,§] and Surya Prakash Singh[*,†,‡]

[†]Polymers and Functional Materials Division, CSIR-Indian Institute of Chemical Technology, Uppal Road, Tarnaka, Hyderabad, 500007, India

[‡]Academy of Scientific and Innovative Research (AcSIR), New Delhi, 110001, India

[§]CSIR-National Physical Laboratory, New Delhi, 110012, India

Supporting Information

ABSTRACT: A new benzofuran-derived fulleropyrrolidine derivative denoted as FB-C_{60} is synthesized by Prato single step synthetic protocol and successfully utilized as an electron acceptor in the bulk heterojunction organic solar cells (OSCs). The molecule possesses significant optoelectronic and redox properties, which are compatible with popular polymer donors. The OSCs constructed from PTB7/FB-C_{60} blends yielded a highest power conversion efficiency (PCE) of 8.1%. The champion device that was fabricated from PTB7-Th/FB-C_{60} bulk-composite film demonstrated a PCE of 9.6%, open circuit voltage of 0.83 V, series resistance of 3.3 $\Omega \cdot cm^{-2}$ and 75.1% of external quantum efficiency at 640 nm wavelength. A promising electron mobility of 1.2×10^{-3} cm^2 V^{-1} s^{-1} of FB-C_{60} is observed in the fabricated device. FB-C_{60} shows the potential to positively replace the conventional PCBM to fabricate "cost-effective" high-performance OSCs.

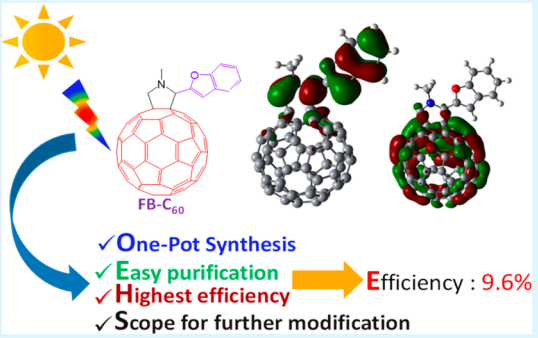

KEYWORDS: *benzofuran-based electron acceptor, one-pot synthesis, bulk-heterojunction organic solar cells, high efficiency, electron mobility*

1. INTRODUCTION

The demand for renewable energy resources has gained immense attention in the global energy outlook ever in the past to deal with the problems associated with fossil fuels, such as their limited storage and adverse impact on the environment. In this context, organic photovoltaic (OPV) technology has gained the limelight of research interest due to their several attractive features, such as lightweight, flexibility, roll-to-roll printing, multiple synthetic approaches, and so forth.[1−8] Since the beginning of the OPV technology, several researchers put their efforts to push the power conversion efficiency (PCE) of solar cells. As time passes, different types of solar cells came across in this field and recently the single and tandem solar cells have attracted good attention due to their high PCE over 14−15%.[9,10] However, the bulk heterojunction (BHJ) organic solar cells (OSCs) have gained significant potential based on three-dimensional interpenetrating network of electron donor and acceptor, which ensures a large interfacial area for efficient exciton dissociation, and thus facilitates the charge generation and subsequently collection at the respective electrodes through percolation path.[11−13] The PCE of BHJ-OSCs has reached over 10% with the invention of new promising donor molecules, particularly low band gap polymers.[14−16] Although several research works have been carried out to synthesize new donor materials for OPV application, very few reports are available on the synthesis of new fullerene derivatives as acceptors. So far, [6,6]-phenyl-C_{61}-butyric acid methyl ester ($PC_{61}BM$) appeared to be the most popular choice as electron acceptor for BHJ OSC fabrication due to their high electron affinity, good electron mobility. and excellent compatibility with commonly used electron donors.[17] However, $PC_{61}BM$ also have the drawbacks such as weak absorption (limited in the UV-region) and nanoscale phase segregation in film, which accelerates the degradation of photoactive layer and thus reduces durability of the device.[18,19] In addition, $PC_{61}BM$ forms a large lowest unoccupied molecular orbital (LUMO) energy offset with polymer donors leading to loss of photon energy during the photoinduced electron transfer.[20] Moreover, synthesis of methano and diarylmethano fullerene derivatives

Received: July 2, 2018
Accepted: January 8, 2019
Published: January 8, 2019

DOI: 10.1021/acsaem.8b01064
ACS Appl. Energy Mater. 2019, 2, 1019−1025

(PCBMs) is a challenging task due to their multistep synthesis, low yields, and difficulty in large scale production.

Our group is fascinated in designing and the synthesis of fulleropyrrolidine derivatives by facile single step synthetic protocol with high purity and yield to overcome the drawbacks associated with PCBM. The fulleropyrrolidine derived acceptors have stable nature under ambient temperature compared to PCBM derivatives due to the formation of 5-membered heterocyclic pyrrolidine ring in fulleropyrrolidines. Different types of analogues are also easy to prepare in large-scale within a short span of time. The fulleropyrrolidine derivatives were first reported by Prato and co-workers in 1993 by using 1,3-dipolar azomethine ylides and fullerene(C_{60}).[21] Wilson et al. later on reported N-unsubstituted fulleropyrrolidine derivatives, which were readily obtained by one-pot synthesis from the reaction of fullerene and azomethine ylides, which were generated from aldehydes and amino acids through decarboxylation and dehydration process.[22] The fulleropyrrolidine derivatives have several advantages over their counterparts such as, (i) a wide variety of starting materials, that is, α-amino acids and aldehydes are readily available, (ii) reaction leads to single mono addition compound, (iii) two functional groups can be introduced simultaneously, and (iv) the obtained compounds are thermally stable. The fulleropyrrolidine derivatives exhibit singlet and excited triplet state properties, which are distinct from the properties of pristine C_{60}. Addition of functionalization groups improves the photophysical and electrochemical characteristics of C_{60} further.[23] Because of these attractive features, several research groups have developed fulleropyrrolidine-derived acceptors for OPV application. Huang and co-workers have synthesized new fulleropyrrolidine derivatives via Prato reaction. The OSCs constructed from those acceptors blending with P3HT donor exhibited a PCE of 2.8%.[24] Zhang et al. developed self-organized fulleropyrrolidine derivatives by facile drop casting method which forms flower-like supramolecular assembly having practical applications in organic electronics.[25]

In OSCs, most of the molecules have been derived by thiophene analogues as major units, however, the recent research in OSCs based on benzofuran unit has also attracted significant interest in the field of OPV. In this context, the small atomic size of oxygen atom in the bezofuran compared to the size of a sulfur atom in the thiophene unit will help in the decrease of steric hindrance to the next adjacent unit.[26] The electronegative oxygen atom also favorably influences the frontier molecular orbital (FMO) energy levels of the resultant molecule forming extended π-conjugated structures.[27] Molecules containing benzofuran show good solubility in readily available organic solvents and hence form smooth morphology in thin films coated from those solutions. Benzofuran moiety has been earlier utilized to develop low band gap donor molecules replacing the commonly used thiophene unit.[28] Here, for the first time we report a new benzofuran-derived fulleropyrrolidine derivative, synthesized using single step synthetic protocol and coded as FB-C_{60}, as an electron acceptor in BHJOSCs. Two popular polymer donors—poly[[4,8-bis[(2-ethylhexyl)oxy]benzo[1,2-b:4,5-b']-dithiophene-2,6-diyl][3-fluoro-2-[(2-ethylhexyl)carbonyl]-thieno[3,4-*b*]thiophenediyl]] (PTB7) and poly[4,8-bis(5-(2-ethylhexyl)thiophen-2-yl)benzo[1,2-b;4,5-b′]dithiophene-2,6-diyl-*alt*-(4-(2-ethylhexyl)-3-fluorothieno[3,4-*b*]thiophene-)-2-carboxylate-2−6-diyl)] (PTB7-Th) have been independently used to fabricate the OPV devices. PTB7-Th/FB-C_{60} and PTB7/FB-C_{60} shows the high PCEs of 9.6 and 8.1% in OSCs, respectively. A comparative study with $PC_{61}BM$ on optical, electrochemical, and photovoltaic properties has been systematically presented here.

2. EXPERIMENTAL DETAILS

2.1. Synthesis. *Synthesis of FB-C_{60}(N-Methyl-2-[benzofuran-2-] fulleropyrrolidine).* One hundred milligrams of fullerene-C_{60} (0.132 mmol) was dissolved in 20 mL of dry toluene in a round-bottomed flask. Further, benzofuran-2-carboxaldehyde (19.29 mg, 0.132 mmol) and *N*-methylglycine (117 mg, 1.315 mmol) were added to the previous solution and refluxed at 110 °C for 24 h. Thereafter, the reaction mixture was cooled down to room temperature and filtered, the solvent was removed under reduced pressure, and finally the residue was subjected to column chromatography (silica gel; hexane/ethyl acetate, 9:1), which afforded the compound FB-C_{60} as a brown solid (43% yield, and it is 72% based on the recovery of unreacted C_{60}). The reaction was optimized at different conditions by varying the temperature and time. At vigorous conditions and prolonged time, we have observed that formation of multiadducts (monitored by TLC) in trace amount leads to less yields and also decreased reaction time (12 h) leads to less conversion rate of reaction of only 30%. Finally we have concluded that 24 h reaction with respective temperature is the optimized condition to get desired product.The spectral graphs of NMR and MS are provided in the Supporting Information (Figures S1 and S2). Scheme 1 depicts the simple one step synthetic protocol of FB-C_{60}. ^{1}H NMR (500 MHz, $CDCl_3$,δ): 7.64−7.59 (dd, J = 2.7 Hz, J = 1.13 Hz 1H), 7.57−7.50 (d, J = 7.7 Hz 1H), 7.32−7.27 (dd, 1H), 7.25−7.21 (dd, 1H), 7.15 (s 1H), 5.26 (s, 1H), 5.08−5.01 (d, J = 9.4 Hz 1H), 4.34−4.28 (d, J = 9.4 Hz 1H), 2.93 (s, 3H). ^{13}C NMR (300 MHz, $CDCl_3$): 40.33, 69.22, 69.93, 75.70, 108.22, 111.69, 121.28, 123.07, 124.24, 140.07, 140.17, 140.24, 142.07, 142.17, 142.61, 144.40, 145.30, 145.44, 145.59, 145.68, 146.00, 146.16, 146.25, 147.37, 152.91. HRMS: $C_{71}H_{11}NO$ calcd (m/z), 894.10; found, 894.09 (m/z). CHNS: $C_{71}H_{11}NO$ calcd, C 95.40, H 1.24, N 1.57, O 1.79; found, C 95.01, H 1.16, N 1.50.

Scheme 1. For Synthesis of FB-C_{60}, the Fullerene Is Subjected to *N*-Methyl Glycine and Benzofuran-2-Carboxaldehyde in Toluene and Refluxed at 110 °C for 24 h

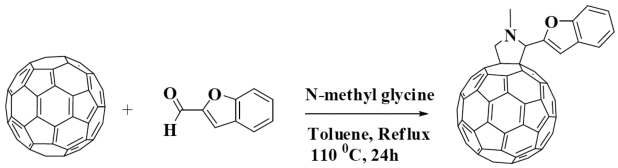

2.2. Device Fabrication. *Preparation of ZnO Sol−Gel.* Zinc acetate dihydrate [$Zn(CH_3COO).2H_2O$] (Aldrich, 99.9%) with 0.1 M concentration was first dissolved in anhydrous ethanol (99.5+ %, Aldrich) and rigorously stirred for 2−3 h at 80 °C. Subsequently, ethanolamine was added to the solution as sol stabilizer followed by thorough mixing process with magnetic stirrer for 12−15 h at 60 °C.[29]

Fabrication of Solar Cells. The indium tin oxide (ITO) coated glass substrates with sheet resistance of ∼12 Ω/□ were first patterned by photolithography to prepare bottom electrode, that is, cathode. The substrates were then thoroughly cleaned with standard RCA-II solution.[30,31] Thereafter the substrates were treated with UV-ozone for 20 min to remove contaminants, if any. The prepared ZnO sol−gel was spin coated on the ITO substrate at 3000 rpm and subsequently heated at 200 °C for 15 min in air to obtain a thickness of ∼30 nm.[32] On the top of ZnO layer, the photoactive layer (PTB7 and PTB7-Th) was spin coated at 90 nm and dried at 40 °C for 1 h, 10 nm thick molybdenum oxide (MoO_3) was deposited by thermal evaporation at a rate of 0.1−0.2 Å·s^{-1}, and finally, 85 nm thick silver (Ag) was deposited at a rate of 0.5−1.0 Å·s^{-1} to form the anode in a vacuum deposition system with a base pressure below 5 × 10^{-6} mbar.

DOI: 10.1021/acsaem.8b01064
ACS Appl. Energy Mater. 2019, 2, 1019−1025

Figure 1 schematically depicts the device architecture and energy level diagram of the solar cell, respectively. The thicknesses of different

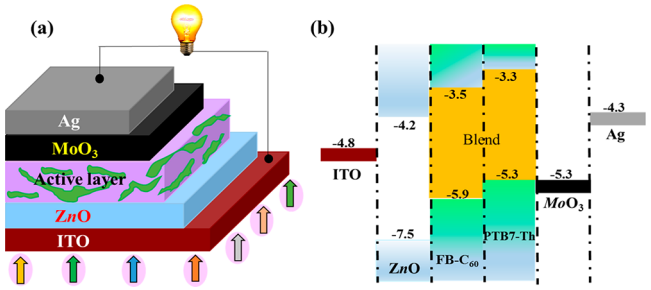

Figure 1. (a) Cross-sectional view of a typical inverted structure BHJ solar cell made from PTB7/FB-C_{60} blends. (b) Energy level diagram of the corresponding solar cell. All energy values are in eV unit.

constituent layers are mentioned in the schematic. The energy values of ITO, ZnO, PTB7, MoO_3, and Ag have been collected from the literatures.[33]

2.3. Device Characterization. A xenon arc lamp-based Newport's Oriel solar simulator (1000 W) was used as a light source for photovoltaic measurements and the intensity of incident light was kept at 100 mW/cm^2. Current density−voltage (J−V) characteristics of the devices were measured with a Keithley 2400 electrometer which shines light with AM 1.5 G spectral distribution and was calibrated using a certified reference solar cell to an intensity of 100 mW/cm^2. A shadow mask with aperture of 10 mm^2 was used to fix the device area. The external quantum efficiency (EQE) was measured with a lock-in detector after illuminating the device area with a monochromatic light of different wavelengths.

3. RESULTS AND DISCUSSION

3.1. UV−visible Absorption. Figure 2 depicts the absorption profile of FB-C_{60} and $PC_{61}BM$ in dichloromethane

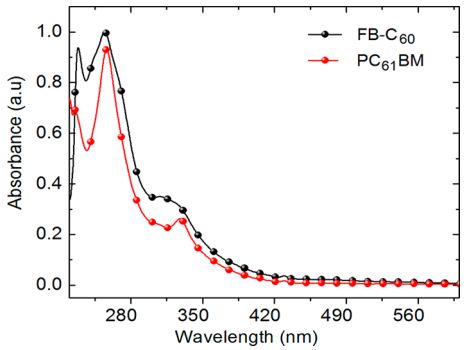

Figure 2. UV−visible absorption spectrum of FB-C_{60} in comparison with standard $PC_{61}BM$ in dichloromethane.

at concentration of 10^{-5} M. The absorption coefficient of FB-C_{60} is higher in comparison to $PC_{61}BM$. Both molecules possess two shoulder peaks in the range of 220−280 nm due to fullerene moiety. In comparison to $PC_{61}BM$, a new broad peak was observed at 300−350 nm for FB-C_{60} that corresponds to the attachment of the benzofuran unit to the fullerene C_{60}. A weak peak at 430 nm is also observed in the both FB-C_{60} and $PC_{61}BM$.[34,35] Further, we also recorded the thin film absorption of both molecules and show the red shift in the 300−350 nm and also the broad shift at 400−500 nm shown in Figure S5.

3.2. Electrochemical Properties. The electrochemical properties of constituent molecules are crucial for efficient charge separation and transport in an OSC. To estimate the FMO energy levels viz., highest occupied molecular orbital (HOMO) and LUMO energy levels of the new molecule, we have conducted cyclic voltammetric (CV) measurements in *o*-dichlorobenzene using ferrocene as the internal standard (Figure S7). FB-C_{60} displays three reversible reduction waves in the potential window of 0 to −2.0 V, which are more like $PC_{61}BM$ shown in Figure 3.[35] The HOMO and LUMO energy levels are determined from the potential (V) versus Fc/Fc^+ plot by using following equation

$$E_{LUMO} = -E_{red}^{Fc/Fc+} + 4.8 \quad (1)$$

$$E_{HOMO} = -E_{ox}^{Fc/Fc+} + 4.8 \quad (2)$$

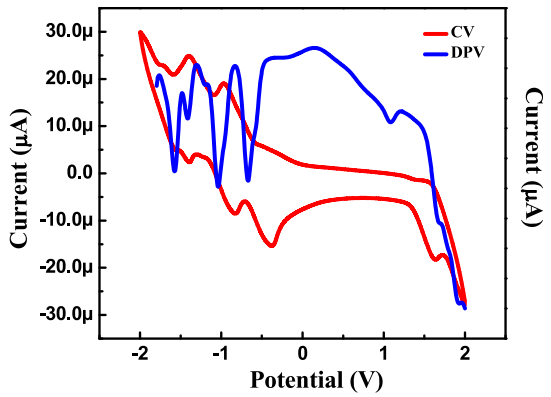

Figure 3. Cyclic voltammetry of FB-C_{60}.

The $E_{(ferrocene)}^{onset}$ of 0.54 is taken as the standard for calculating HOMO and LUMO.[36,37] The LUMO and HOMO values of FB-C_{60} are found to be −3.58 and −5.91 eV, respectively, which are commensurable with most of the donor polymer's FMO energy levels for charge transfer. A comparatively low lying LUMO energy level of FB-C_{60} (−3.58 eV) is expected to show higher open circuit voltage in device with respect to PCBM, which is having a LUMO value of −3.60 eV (Table 1).

Table 1. HOMO and LUMO Values of FB-C_{60} and $PC_{61}BM$

acceptor	E^1_{red} (V)	E^1_{ox} (V)	E_{LUMO} (eV)	E_{HOMO} (eV)
$PC_{61}BM$	−0.66	1.68	−3.60	−5.94
FB-C_{60}	−0.68	1.65	−3.58	−5.91

3.3. DFT Calculation. To get an intuitive idea about the electronic distribution of FMO energy levels associated with FB-C_{60}, quantum-chemical calculations were performed based on density functional theory[38] using Gaussian software package after the ab-initio structure optimization. Becke−Lee−Yang−Parr hybrid exchange correlation three parameter functional (B3LYP)[39,40] and 6-311G (d, p) basis set have been used for the self-consistent-field (SCF) calculation. Dichloromethane (DCM) phase, single spin, and tight convergence are selected as parameters. The DFT calculations of optimized structures have given in the supporting file (Supporting Information S6). As can be seen from Figure 4, in HOMO the electron density is concentrated on the pyrrolidine and furan unit where, as in the LUMO, the electron density is uniformly distributed over the entire fullerene unit. The fullerene units are more sterically

DOI: 10.1021/acsaem.8b01064
ACS Appl. Energy Mater. 2019, 2, 1019−1025

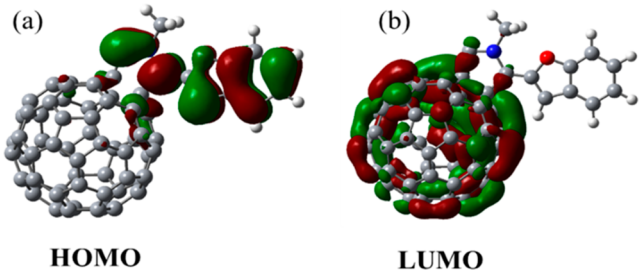

Figure 4. Electron distributions of (a) HOMO and (b) LUMO associated with FB-C_{60} as calculated by density functional theory using B3LYP/6-3111 g(d, p)as basis set.

available to the polymer donors in a blend, hence this kind of electronic configuration is expected to favor charge transfer from donor to the acceptor. The simulated absorption profile of FB-C_{60} in DCM also closely resembles the spectrum that was obtained from experimental measurements as is shown in the Supporting Information Figure S6.

3.4. Light *J*–*V* Characteristics. To investigate the photovoltaic performance of new fullerene acceptor FB-C_{60}, OPV devices were fabricated in inverted structure according to following configuration-ITO/ZnO/photoactive blend layer/MoO_3/Ag. Two popular conjugated polymers PTB7 and PTB7-Th were independently used as electron donor materials to check if there any dependency of device performance on the choice of donors. Reference solar cells were made from PTB7/$PC_{61}BM$ and PTB7-Th/$PC_{61}BM$ bulk composite films in the same experimental conditions. Reference cells using $PC_{71}BM$ as an acceptor and PTB7-Th as donor were also constructed for further comparison. For optimization of device performance, initially solar cells were made with three different donor-to-acceptor weight ratios, and in the next step different annealing temperatures were tried out to improve the morphology of photoactive layer by keeping the optimized *D*/*A* ratio fixed. From an experiment of varying *D*/*A* weight ratio (1:1, 1:1.5, and 1:2), the *D*/*A* weight ratio of 1:1.5 is found to be optimum for this combination of molecules (Figure S3). Thermal annealing treatment of photoactive layer at 40 °C for an hour resulted in best photovoltaic performance of the devices (Figure S4).

Figure 5 shows the characteristics *J*–*V* curves of the best performing solar cells from each category measured under 1 sun illumination, that is, 100 mW·cm^{-2} light intensity. The PTB7/FB-C_{60} based OSCs showed a highest PCE of 8.1% V_{oc} of 0.773 V, J_{sc} of 16.0 mA·cm^{-2} and ff of 65.5%. On the other hand, PTB7/$PC_{61}BM$ based reference cells yielded a maximum efficiency of 7.2% (V_{oc} = 0.77 V, J_{sc} = 16.8 mA·cm^{-2} and ff = 0.56). The champion device made from PTB7-Th/FB-C_{60} blend exhibited a PCE of 9.6% with V_{oc} of 0.833 V, J_{sc} of 17.1 mA·cm^{-2} and ff of 0.68. The reference cell made from PTB7-Th/$PC_{61}BM$ composite film fabricated from the same run showed a PCE of 7.6%, whereas PTB7-Th/$PC_{71}BM$ based reference cell demonstrated a highest PCE of 8.9% with V_{oc} of 0.8 V, J_{sc} of 16.6 mA·cm^{-2} and ff of 0.67. All the photovoltaic parameters are summarized in Table 2. It is noteworthy to mention that OSCs made from new acceptor FB-C_{60} showed comparatively less series resistances (R_s) than the PCBM-based devices. This is probably due to improved film morphology and better metal–semiconductor interface in the case of FB-C_{60} based devices. In contrast, shunt resistance (R_{sh}) is found to be poor in our devices indicating more charge

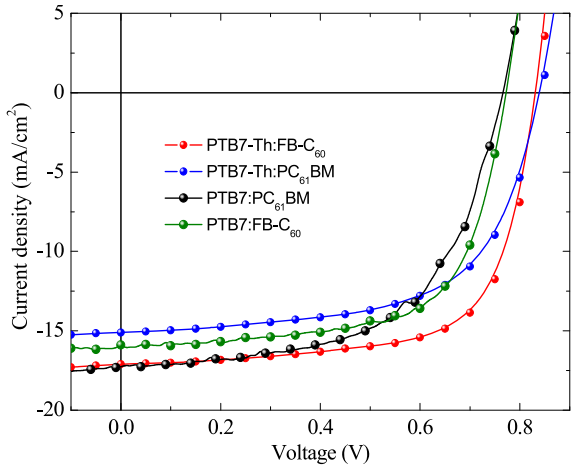

Figure 5. Light *J*–*V* characteristics of new fullerene FB-C_{60} based devices. PTB7 and PTB7-Th are used as electron donors. $PC_{61}BM$ was used as acceptor in reference samples.

recombination in these categories of devices. It also hints about scopes to improve the device performance further by proper optimization process. Statistical device data has given in the Supporting Information Table S11.

3.5. External Quantum Efficiency. The external quantum efficiency (EQE), which is defined as the ratio of collected electron to incident photon at a wavelength, informs about spectral dependence of the energy conversion process in a solar cell. Figure 6 demonstrates the EQE spectra of best performing solar cells from each category. The EQE value at a given wavelength was calculated by the following relation

$$\mathrm{EQE}(\lambda) = 1240\left(\frac{J_{sc}}{q\lambda P_o}\right) \quad (3)$$

where λ (nm) and P_o (W·m^{-2}) are the wavelength and intensity of incident radiation from monochromator, whereas J_{sc} (mA·cm^{-2}) is the short-circuit photocurrent density as measured by lock-in-amplifier. The PTB7/FB-C_{60} based OSCs showed a highest EQE value of 64.4% at 625 nm. A flat region in the EQE spectrum is observed in the wavelength range of 600–678 nm. The champion device from PTB7-Th/FB-C_{60} category showed a highest EQE of 75.1% at 640.7 nm. On the other hand, the reference solar cells made from PTB7-Th/$PC_{61}BM$ blend showed an optimum EQE of 67.6% for the wavelength range of 648–700 nm. The J_{sc} value obtained by integrating the EQE spectrum overlapping with AM 1.5G solar irradiance ϕ (λ) in the wavelength range from 300 to 900 nm using the following expression,

$$J_{sc} = q\int \mathrm{EQE}(\lambda)\varphi(\lambda)\mathrm{d}\lambda \quad (4)$$

matches well with the J_{sc} values measured during light *J*–*V* characterization.

3.6. Mobility Measurements. The charge carrier mobility of electron donor and acceptor materials plays crucial roles in controlling photovoltaic performance of photovoltaic devices. In order to estimate the electron mobility (μ_e) of acceptors, "electron-only" devices were made with the structure ITO/ZnO/active layer/Al. Similarly, "hole-only" devices with configuration ITO/PEDOT:PSS/active layer/*Au* were constructed to measure the hole mobility (μ_h) of PTB7-Th. The

DOI: 10.1021/acsaem.8b01064
ACS Appl. Energy Mater. 2019, 2, 1019–1025

Table 2. Photovoltaic Parameters of Proto-Type Photovoltaic Devices Prepared from FB-C_{60} Using PTB7 and PTB7-Th as Electron Donors

donor	acceptor	V_{oc} (V)	J_{sc} (mA/cm^2)	ff (%)	PCE (%)	R_{sh} (kΩ·cm^{-2})	R_s (Ω·cm^{-2})
PTB7	FB-C_{60}	0.773	16.0	65.5	8.1	404.7	5.14
	$PC_{61}BM$	0.77	16.8	56.0	7.2	434.8	7.11
PTB7-Th	FB-C_{60}	0.833	17.1	67.5	9.6	723.8	3.31
	$PC_{61}BM$	0.841	15.1	60.0	7.6	765.2	5.98
	$PC_{71}BM$	0.800	16.6	67.2	8.9	712.5	4.11

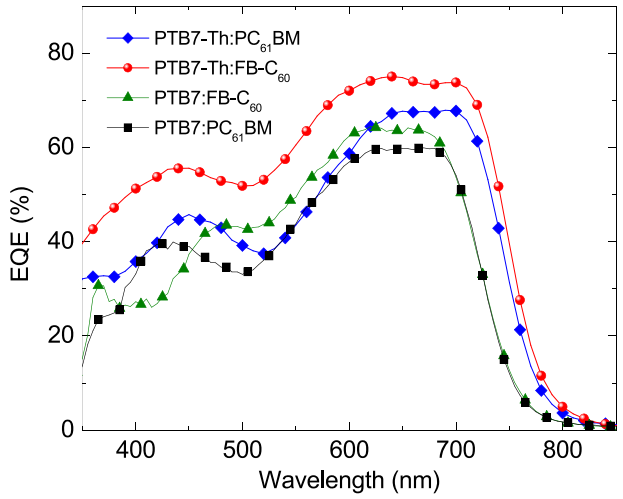

Figure 6. EQE spectra of FB-C_{60} based OPV devices in comparison with reference cells. Two popular polymer donors PTB7 and PTB7-Th have been independently used to form the photoactive blend layer.

energy level diagrams of corresponding devices are shown in Figure 7a,b, respectively.

The dark current density−voltage (J−V) characteristics of the respective devices were fitted with Mott−Gurney's space-charge-limited-current (SCLC) model at higher voltages where charge transport is controlled by accumulated space charges and obeys following relation[41]

$$J = \frac{9\varepsilon_o\varepsilon_r\mu V^2}{8d^3} \quad (5)$$

Here, ε_o is free-space permittivity, ε_r is relative permittivity, and d is the film thickness. The electron mobility of FB-C_{60} in blend active layer is calculated to be 1.2 × 10^{-3} cm^2·V^{-1}·s^{-1}, which is much higher compared to that of $PC_{61}BM$ estimated to be 5.1 × 10^{-4} cm^2·V^{-1}·s^{-1}. $PC_{71}BM$ is found to have a μ_e value of 9.3 × 10^{-4} cm^2·V^{-1}·s^{-1}. However, hole mobility is found to be in the range of 1.3−1.6 × 10^{-4} cm^2·V^{-1}·s^{-1} for all three blends. The μ_h and μ_e values of respective devices are tabulated in Table 3. It is important to note that the hole and electron mobility are more well-balanced in the case of PTB7-Th/FB-C_{60} blends compared to other blends under investigation. A balanced charge transport property of hole and electron is known to help in improving the fill factor in the OPV devices, which is in agreement with our device results.

Table 3. Electron Mobility of FB-C_{60} in Comparison with Conventional $PC_{61}BM$ and $PC_{71}BM$ in their Respective Blend Films with PTB7-Th

acceptor	μ_h (cm^2 V^{-1} s^{-1})	μ_e (cm^2 V^{-1} s^{-1})	ratio
$PC_{61}BM$	1.3 × 10^{-3}	5.1 × 10^{-4}	2.5
$PC_{71}BM$	1.6 × 10^{-3}	9.3 × 10^{-4}	1.7
FB-C_{60}	1.5 × 10^{-3}	1.2 × 10^{-3}	1.2

3.7. Morphology Study. The surface morphology of the blend films was investigated by atomic force microscopy and grazing incident X-ray diffraction spectroscopy (GIXRD). Figure 8a,d shows the topological images of PTB7:$PC_{61}BM$ and PTB7/FB-C_{60} films, respectively, for a scanning area of 5 μm × 5 μm. The PTB7/$PC_{61}BM$ (2:3 w/w) blend films showed an average root-mean-square (RMS) roughness of 7.1 nm, whereas the PTB7/FB-C_{60} based films annealed at 40 °C showed an RMS value of only 5.7 nm for a blend ratio of 2:3. The three-dimensional views of the films are demonstrated in Figure 8b,e. Figure 8c,f illustrates the phase images. A film surface with comparatively less roughness is known to promote the charge collection (η_{cc}) by improving the metal−semiconductor interface in the case of device. GIXRD curves of the films (Figure S10) do not show any notable difference. Therefore, an increase in the electron mobility may be the

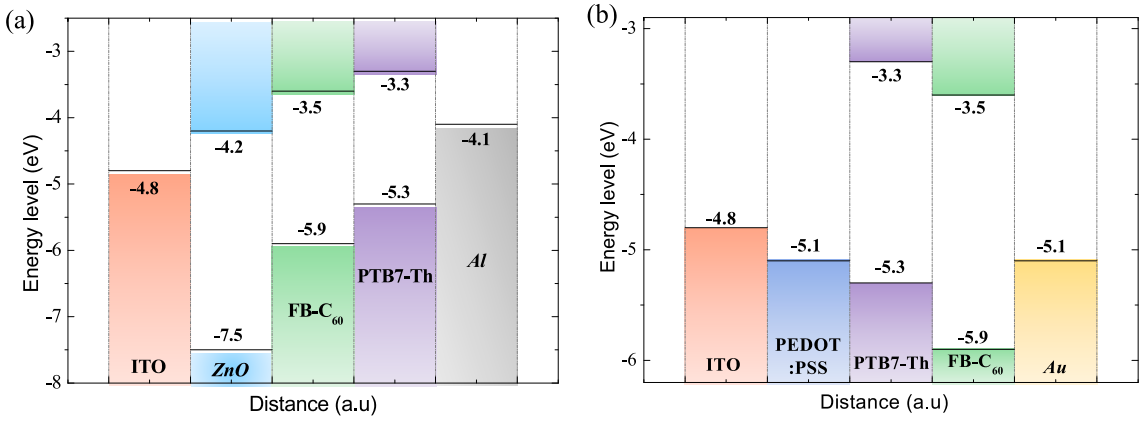

Figure 7. Energy level diagrams of (a) electron-only and (b) hole-only devices.

DOI: 10.1021/acsaem.8b01064
ACS Appl. Energy Mater. 2019, 2, 1019−1025

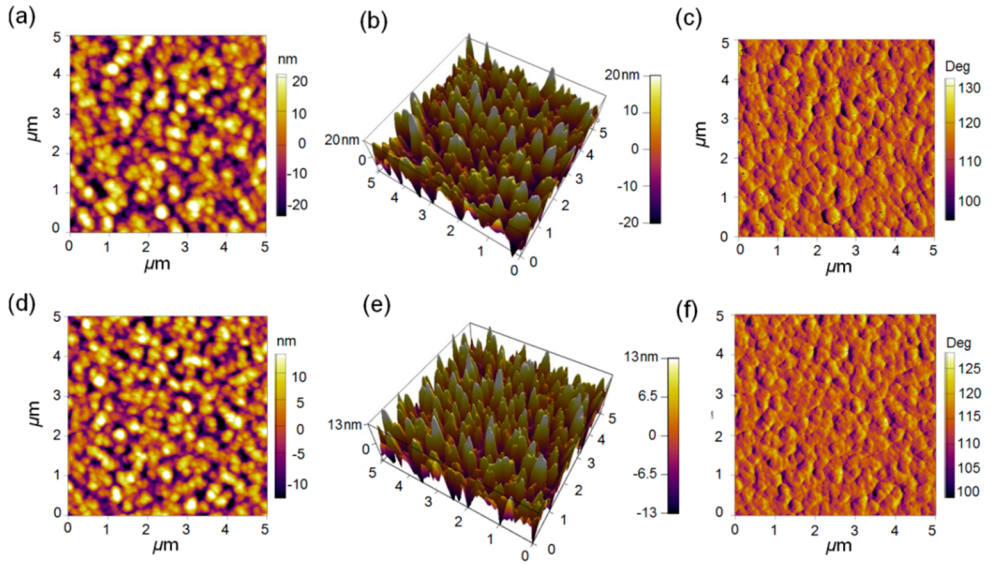

Figure 8. Atomic force microscopic images of (a–c) PTB7/$PC_{61}BM$ and (d–f) PTB7/FB-C_{60} bulk composite films coated on ITO coated glass substrates.

main reason for performance increase. Hence, PCE of the OSC is desired to be more, which matches with photovoltaic results as reported in Figure 5. The solar cell stability was done in air without encapsulation. The results are shown in Figure S11, the FB-C60 based solar cells are more stable over a long period of time.

4. CONCLUSION

A new fulleropyrrolidine derivative labeled as FB-C_{60} has been synthesized by a simple one-pot synthetic protocol for use in OSC as the electron acceptor. The molecule has LUMO and HOMO energy levels at −3.59 and −5.90 eV, respectively, which are compatible with popular polymer donor materials, such as PTB7 and PTB7-Th. The OSCs made from PTB7/FB-C_{60} blend demonstrated a high PCE of 8.1% in optimized conditions, whereas the champion device fabricated from PTB7-Th/FB-C_{60} blend showed a PCE of 9.6%. The reference solar cells constructed from PTB7/$PC_{61}BM$ and PTB7-Th/$PC_{61}BM$ bulk-composite films showed maximum PCEs of 7.2 and 7.6%, respectively. A high EQE of about 75% was observed for PTB7-Th/FB-C_{60} based solar cells in the wavelength region of 612–702 nm. FB-C_{60} showed a promising electron mobility of 1.2×10^{-3} $cm^2 \cdot V^{-1} \cdot s^{-1}$ in PTB7-Th/FB-C_{60} blend films, which is comparable to the hole mobility of donor molecule. The active layers made from FB-C_{60} also showed smooth film morphology with RMS roughness of only 5.7 nm, which is beneficial for charge collection. Hence, FB-C_{60} having attractive electrochemical and electronic properties can be conveniently used as a replacement of PCBM to fabricate low-cost OSCs.

■ ASSOCIATED CONTENT

Supporting Information

The Supporting Information is available free of charge on the ACS Publications website at DOI: 10.1021/acsaem.8b01064.

Detailed description regarding structural characterization by ^1H NMR, HRMS, optimization of device performance, thin film absorption, ferrocene–CV, DFT studies, GIXRD data, and solar cell device stability (PDF)

■ AUTHOR INFORMATION

Corresponding Author

*E-mail: spsingh@iict.res.in.

ORCID

Surya Prakash Singh: 0000-0001-5670-7329

Notes

The authors declare no competing financial interest.

■ ACKNOWLEDGMENTS

P.N. thanks the CSIR, Government of India for providing SRF. S.P.S. gratefully acknowledges SUNRISE and Indo-Poland Project DST/INT/POL/P-26/2016 for financial support.

■ REFERENCES

(1) Günes, S.; Neugebauer, H.; Sariciftci, N. S. Conjugated Polymer-Based Organic Solar Cells. *Chem. Rev.* **2007**, *107*, 1324–1338.

(2) Walker, B.; Kim, C.; Nguyen, T.-Q. Small Molecule Solution-Processed Bulk Heterojunction Solar Cells. *Chem. Mater.* **2011**, *23*, 470–482.

(3) Scharber, M. C.; Sariciftci, N. S. Efficiency of Bulk-heterojunction Organic Solar Cells. *Prog. Polym. Sci.* **2013**, *38*, 1929–1940.

(4) Liu, Y.; Zhao, J.; Li, Z.; Mu, C.; Ma, W.; Hu, H.; Jiang, K.; Lin, H.; Ade, H.; Yan, H. Aggregation and Morphology Control Enables Multiple Cases of High-efficiency Polymer Solar Cells. *Nat. Commun.* **2014**, *5* (1–10), 5293.

(5) Cui, C.; Guo, X.; Min, J.; Guo, B.; Cheng, X.; Zhang, M.; Brabec, C. J.; Li, Y. High-Performance Organic Solar Cells Based on a Small Molecule with Alkylthio-Thienyl-Conjugated Side Chains without Extra Treatments. *Adv. Mater.* **2015**, *27*, 7469–7475.

(6) Kan, B.; Li, M.; Zhang, Q.; Liu, F.; Wan, X.; Wang, Y.; Ni, W.; Long, G.; Yang, X.; Feng, H.; Zuo, Y.; Zhang, M.; Huang, F.; Cao, Y.; Russell, T. P.; Chen, Y. A Series of Simple Oligomer-like Small Molecules Based on Oligothiophenes for Solution-Processed Solar Cells with High Efficiency. *J. Am. Chem. Soc.* **2015**, *137*, 3886–3893.

(7) Savagatrup, S.; Printz, A. D.; O'Connor, T. F.; Zaretski, A. V.; Rodriquez, D.; Sawyer, E. J.; Rajan, K. M.; Acosta, R. I.; Root, S. E.; Lipomi, D. J. Mechanical Degradation and Stability of Organic Solar Cells: Molecular and Microstructural Determinants. *Energy Environ. Sci.* **2015**, *8*, 55–80.

(8) Lucera, L.; Machui, F.; Kubis, P.; Schmidt, H. D.; Adams, J.; Strohm, S.; Ahmad, T.; Forberich, K.; Egelhaaf, H. J.; Brabec, C. J.

DOI: 10.1021/acsaem.8b01064
ACS Appl. Energy Mater. 2019, 2, 1019–1025

Highly Efficient, Large Area, Roll Coated Flexible and Rigid OPV Modules with Geometric Fill Factors up to 98.5% Processed with Commercially Available Materials. *Energy Environ. Sci.* **2016**, *9*, 89−94.
(9) Zhang, Y.; Kan, B.; Sun; Wang, Y.; Xia, R.; Ke, X.; Yi, Y-Q-Q.; Li, C.; Yip, H.; Wan, X.; Cao, Y.; Chen, Y. Nonfullerene Tandem Organic Solar Cells with High Performance of 14.11%. *Adv. Mater.* **2018**, *30* (1−7), 1707508.
(10) Li, N.; Baran, D.; Forberich, K.; Machui, F.; Ameri, T.; Turbiez, M.; Carrasco-Orozco, M.; Drees, M.; Facchetti, A.; Krebs, F. C.; Brabec, C. J. Towards 15% Energy Conversion Efficiency: a Systematic Study of the Solution-Processed Organic Tandem Solar Cells Based on Commercially Available Materials. *Energy Environ. Sci.* **2013**, *6*, 3407−3413.
(11) Sariciftci, N. S.; Braun, D.; Zhang, C.; Srdanov, V. I.; Heeger, A. J.; Stucky, G.; Wudl, F. Semiconducting Polymer buckminsterfullerene Heterojunctions: Diodes, Photodiodes, and Photovoltaic Cells. *Appl. Phys. Lett.* **1993**, *62*, 585−587.
(12) Yu, G.; Gao, J.; Hummelen, J. C.; Wudl, F.; Heeger, A. J. Polymer Photovoltaic Cells: Enhanced Efficiencies *via* a Network of Internal Donor-Acceptor Heterojunctions. *Science* **1995**, *270*, 1789−1791.
(13) Savenije, T. J.; Warman, J. M.; Goossens, A. Visible Light Sensitisation of Titanium Dioxide Using a Phenylene Vinylene Polymer. *Chem. Phys. Lett.* **1998**, *287*, 148−153.
(14) You, J.; Dou, L.; Yoshimura, K.; Kato, T.; Ohya, K.; Moriarty, T.; Emery, K.; Chen, C.-C.; Gao, J.; Li, G.; Yang, Y. A Polymer Tandem Solar Cell with 10.6% Power Conversion Efficiency. *Nat. Commun.* **2013**, *4* (1), 1446.
(15) Zhang, S.; Ye, L.; Hou, J. Breaking the 10% Efficiency Barrier in Organic Photovoltaics: Morphology and Device Optimization of Well-Known PBDTTT Polymers. *Adv. Energy Mater.* **2016**, *6* (1−20), 1502529.
(16) Zhao, W.; Li, S.; Yao, H.; Zhang, S.; Zhang, Y.; Yang, B.; Hou, J. Molecular Optimization Enables over 13% Efficiency in Organic Solar Cells. *J. Am. Chem. Soc.* **2017**, *139*, 7148−7151.
(17) Hummelen, J. C.; Knight, B. W.; LePeq, F.; Wudl, F.; Yao, J.; Wilkins, C. L. Preparation and Characterization of Fulleroid and Methanofullerene Derivatives. *J. Org. Chem.* **1995**, *60*, 532−538.
(18) Schroeder, B. C.; Li, Z.; Brady, M. A.; Faria, G. C.; Ashraf, R. S.; Takacs, C. J.; Cowart, J. S.; Duong, D. T.; Chiu, K. H.; Tan, C.-H.; Cabral, J. T.; Salleo, A.; Chabinyc, M. L.; Durrant, J. R.; McCulloch, I. Enhancing Fullerene-Based Solar Cell Lifetimes by Addition of a Fullerene Dumbbell. *Angew. Chem., Int. Ed.* **2014**, *53*, 12870−12875.
(19) Wong, H. C.; Li, Z.; Tan, C. H.; Zhong, H.; Huang, Z.; Bronstein, H.; McCulloch, I.; Cabral, J. T.; Durrant, J. R. Morphological Stability and Performance of Polymer−Fullerene Solar Cells under Thermal Stress: The Impact of Photoinduced PC60BM Oligomerization. *ACS Nano* **2014**, *8*, 1297−1308.
(20) Kirchartz, T.; Taretto, K.; Rau, U. Efficiency Limits of Organic Bulk Heterojunction Solar Cells. *J. Phys. Chem. C* **2009**, *113*, 17958−17966.
(21) Maggini, M.; Scorrano, G.; Prato, M. Addition of Azomethine Ylides to C60: Synthesis, Characterization, and Functionalization of Fullerene Pyrrolidines. *J. Am. Chem. Soc.* **1993**, *115*, 9798−9799.
(22) Wilson, S. R.; Wang, Y.; Cao, J.; Tan, X. Amino acids as Precursors for N-Unsubstituted Fulleropyrrolidine Derivatives. *Tetrahedron Lett.* **1996**, *37*, 775−778.
(23) Thomas, K. G.; Biju, V.; George, M. V.; Guldi, D. M.; Kamat, P. V. Excited-State Interactions in Pyrrolidinofullerenes. *J. Phys. Chem. A* **1998**, *102*, 5341−5348.
(24) Ren, B.-Y.; Ou, C.-J.; Zhang, C.; Chang, Y.-Z.; Yi, M.-D.; Liu, J.-Q.; Xie, L.-H.; Zhang, G.-W.; Deng, X.-Y.; Li, S.-B.; Wei, W.; Huang, W. Diarylfluorene-Modified Fulleropyrrolidine Acceptors to Tune Aggregate Morphology for Solution-Processable Polymer/Fullerene Bulk-Heterojunction Solar Cells. *J. Phys. Chem. C* **2012**, *116*, 8881−8887.
(25) Zhang, X.; Nakanishi, T.; Ogawa, T.; Saeki, A.; Seki, S.; Shen, Y.; Yamauchi, Y.; Takeuchi, M. Flowerlike Supramolecular Architectures Assembled from C60 Equipped with a Pyridine Substituent. *Chem. Commun.* **2009**, *46*, 8752−8754.
(26) Huang, P.; Du, J.; Gunathilake, S. S.; Rainbolt, E. A.; Murphy, J. W.; Black, K. T.; Barrera, D.; Hsu, J. W. P.; Gnade, B. E.; Stefan, M. C.; Biewer, M. C. Benzodifuran and Benzodithiophene Donor-Acceptor Polymers for Bulk heterojunction Solar Cells. *J. Mater. Chem. A* **2015**, *3*, 6980−6989.
(27) Walker, B.; Tamayo, A. B.; Dang, X.-D.; Zalar, P.; Seo, J. H.; Garcia, A.; Tantiwiwat, M.; Nguyen, T.-Q. Nanoscale Phase Separation and High Photovoltaic Efficiency in Solution-Processed, Small-Molecule Bulk Heterojunction Solar Cells. *Adv. Funct. Mater.* **2009**, *19*, 3063−3069.
(28) Liu, B.; Chen, X.; Zou, Y.; Xiao, L.; Xu, X.; He, Y.; Li, L.; Li, Y. Benzo[1,2-b:4,5-b′]difuran-Based Donor−Acceptor Copolymers for Polymer Solar Cells. *Macromolecules* **2012**, *45*, 6898−6905.
(29) Kyaw, A. K. K.; Wang, D. H.; Gupta, V.; Zhang, J.; Chand, S.; Bazan, G. C.; Heeger, A. J. Efficient Solution-Processed Small-Molecule Solar Cells with Inverted Structure. *Adv. Mater.* **2013**, *25*, 2397−2402.
(30) Kern, W. The Evolution of Silicon Wafer Cleaning Technology. *J. Electrochem. Soc.* **1990**, *137*, 1887−1892.
(31) Kern, W.; Puotinen, D. A. Radiochetnical Study of Semiconductor Surface Contamination. *RCA Rev.* **1970**, *31*, 187.
(32) Liang, Y.; Xu, Z.; Xia, J.; Tsai, S. T.; Wu, Y.; Li, G.; Ray, C.; Yu, L. For the Bright Future-Bulk Heterojunction Polymer Solar Cells with Power C onversion E fficiency of 7.4%. *Adv. Mater.* **2010**, *22*, E135−E138.
(33) Liu, W.; Li, S.; Huang, J.; Yang, S.; Chen, J.; Zuo, L.; Shi, M.; Zhan, X.; Li, C. Z.; Chen, H. Nonfullerene Tandem Organic Solar Cells with High Open Circuit Voltage of 1.97 V. *Adv. Mater.* **2016**, *28*, 9729−9734.
(34) Saravanan, C.; Liu, C.-L.; Chang, Y.-M.; Lu, J.-D.; Hsieh, Y.-J.; Rwei, S.-P.; Wang, L. [60]Fulleropyrrolidines Bearing π-Conjugated Moiety for Polymer Solar Cells: Contribution of the Chromophoric Substituent on C60 to the Photocurrent. *ACS Appl. Mater. Interfaces* **2012**, *4*, 6133−6141.
(35) Nagarjuna, P.; Bagui, A.; Garg, A.; Gupta, V.; Singh, S. P. One-Step Synthesis of New Electron Acceptor for High Efficiency Solution Processable Organic Solar Cells. *J. Phys. Chem. C* **2017**, *121*, 26615−26621.
(36) Martín, N.; Sánchez, L.; Herranz, M. A.; Guldi, D. M. Evidence for Two Separate One-Electron Transfer Events in Excited Fulleropyrrolidine Dyads Containing Tetrathiafulvalene (TTF). *J. Phys. Chem. A* **2000**, *104*, 4648−4657.
(37) Tian, C.; Castro, E.; Wang, T.; Betancourt-Solis, G.; Rodriguez, G.; Echegoyen, L. Improved Performance and Stability of Inverted Planar Perovskite Solar Cells Using Fulleropyrrolidine Layers. *ACS Appl. Mater. Interfaces* **2016**, *8*, 31426−31432.
(38) Hohenberg, P.; Kohn, W. Inhomogeneous Electron Gas. *Phys. Rev.* **1964**, *136* (3B), B864−B871.
(39) Lee, C.; Yang, W.; Parr, R. G. Development of the Colle-Salvetti Correlation-Energy Formula into a Functional of the Electron Density. *Phys. Rev. B: Condens. Matter Mater. Phys.* **1988**, *37*, 785−789.
(40) Becke, A. D. Density Functional Thermochemistry. III. The Role of Exact Exchange. *J. Chem. Phys.* **1993**, *98*, 5648−5652.
(41) Mott, N. F.; Gurney, R. W. *Electronic Processes in Ionic Crystals*, 1st ed.; Oxford University Press, 1940.

DOI: 10.1021/acsaem.8b01064
ACS Appl. Energy Mater. 2019, 2, 1019−1025